Journal of the Korean Ceramic Society
Vol. 53, No. 3, pp. 312~316, 2016.

http://dx.doi.org/10.4191/kcers.2016.53.3.312

The Effect of Domain Wall on Defect Energetics in Ferroelectric $LiNbO_3$ from Density Functional Theory Calculations

Donghwa Lee†

School of Materials Science and Engineering, Chonnam National University, Gwangju 61186, Korea

(Received April 13, 2016; Revised May 2, 2016; Accepted May 4, 2016)

ABSTRACT

The energetics of defects in the presence of domain walls in $LiNbO_3$ are characterized using density-functional theory calculations. Domain walls show stronger interactions with antisite defects than with interstitial defects or vacancies. As a result, antisite defects act as a strong pinning center for the domain wall in $LiNbO_3$. Analysis of migration behavior of the antisite defects across the domain wall shows that the migration barrier of the antisite defects is significantly high, such that the migration of antisite defects across the domain wall is energetically not preferable. However, further study on excess electrons shows that the migration barrier of antisite defects can be lowered by changing the charge states of the antisite defects. So, excess electrons can enhance the migration of antisite defects and thus facilitate domain wall movement by weakening the pinning effect.

Key words : Defect/Domain wall interaction, Lithium Niobate, Density functional theory

1. Introduction

Ferroelectric materials are of interest for such diverse applications as non-volatile Ferroelectric Random Access Memory (FRAM),[1] electro-optic modulators[2] and frequency converters.[3] Especially, $LiNbO_3$ has excellent piezo- and pyro-electricity properties, is photo-refractive, and displays nonlinear optical properties. It also has a high spontaneous polarization, 70 $\mu C/cm^2$, and high Curie temperature, ~1480 K,[4,5] so it is suitable for high temperature applications as well. Generally, congruent $LiNbO_3$, which has an R3c structure, is easy to grow under Li deficient conditions.[6,7] However, recent successes using the vapor-transport equilibration (VTE) method[8] have enabled the growth of stoichiometric $LiNbO_3$. Although various defect models including those for pseudo-Schottky defects, Schottky defects, and Frenkel defects have been suggested[9] to explain energetically preferred defects and defect clusters in congruent $LiNbO_3$, only an Nb antisite, compensated for by four Li ion vacancies[9-11] and five Nb antisites compensated for by four Nb vacancies[11] were found to successfully explain the stoichiometry of congruent $LiNbO_3$. Atomistic modeling by Donnerberg et al.[12] showed that compensation by Nb vacancies is energetically less favorable than compensation by Li vacancies. Recent DFT calculations[13] showed that Nb antisite compensated for by Li vacancies, and the Li Frenkel pair, are the most energetically favorable defect clusters in $LiNbO_3$ under Li deficient (congruent) and Li rich (stoichiometric) conditions, respectively. An analysis on various Nb antisite-Li vacancy cluster models determined that several arrangements of Li vacancies around an Nb antisite are nearly energetically equivalent.[14]

Interfaces between two opposite polarization domains (Domain walls) are also studied using both experiments and simulations. *Gopalan et al.*[15] suggested two different domain walls, the Y- and X-walls, based on crystallographic orientation; the Y-wall lies parallel to the $(11\bar{2}0)$ plane, while the X-wall lies parallel to the $(10\bar{1}0)$ plane. In subsequent works,[16] the X-wall was identified as a mixed anion-cation plane, while the Y-wall was determined to be alternating planes of cations only and anions only. Energetic studies on the two domain walls[17] show that the Y-wall is energetically favored but less mobile. It was also found that non-uniaxial polarization components near the domain walls can lead to Bloch-like characteristics of the X-wall and both Bloch-like and Néel-like characteristics of the Y-walls.[18] Previous studies have demonstrated that defect/domain wall interactions can lead to switching in the preferred orientation of the domain wall from the Y-wall to the X-wall[19] or to a reduction of the electric polarization.[20] In extending the previous work on defects and domain walls, this study mainly focuses on the interaction between defects and domain walls in $LiNbO_3$ and the effect of those defects on the domain dynamics. Various aspects of defects, including type and charge state, are investigated to understand the effect of domain walls on defect energetics.

2. Simulation Methods

All the calculations are performed within the density functional theory (DFT)[21] level with generalized gradient

†Corresponding author : Donghwa Lee
E-mail : donghwa96@jnu.ac.kr
Tel : +82-62-530-1705 Fax : +82-62-530-1699

approximation[22] of exchange and correlation potential. Monkhorst-Pack[23] k-point sampling with a grid of $1 \times 4 \times 2$ is used. The plane wave DFT calculations are performed with the Vienna *Ab Initio* Simulation Package (VASP)[24,25] using the projected augmented wave (PAW)[26] pseudopotential. The generalized gradient approximation (GGA)[22] is used to evaluate the exchange and correlation interactions. The plane waves are expanded up to 400 eV of kinetic energy.[27] Ionic relaxation is performed until the maximum atomic force is below 0.01 eV/Å. The self-consistent solution of the Kohn-Sham functional is obtained using the residual minimization method direct inversion in the iterative subspace (RMM-DIIS) algorithm,[28] which optimizes several individual energy bands at the same time. The pseudopotential and methodologies used here are the same as those used in our previous studies of intrinsic defects[13] and domain walls.[17] The climbing-image Nudged Elastic Band (NEB) method[29,30] with 10 images is employed to predict the energy barrier of defect migration.

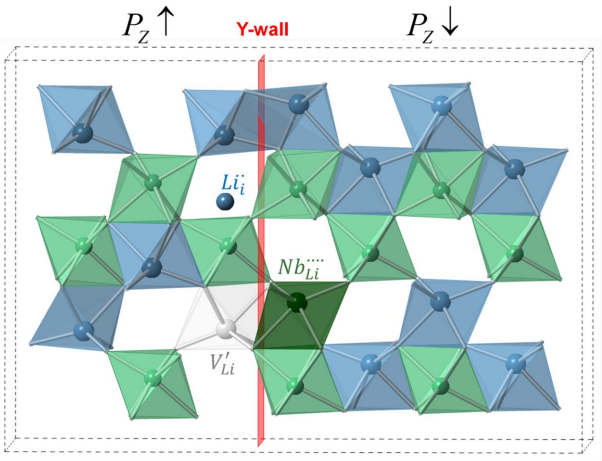

Fig. 1. Schematic view of Y-wall and three major points defects in $LiNbO_3$; $Li_i^{\cdot}$, V_{Li}' and $Nb_{Li}^{\cdot\cdot\cdot\cdot}$ are drawn to show spatial location of each point defect around the Y-wall.

3. Results and Discussion

Although the ferroelectric fatigue and optical instability of ferroelectric $LiNbO_3$ are known to result from defects/domain wall interactions, these drawbacks still limit the usage of ferroelectric materials. To overcome the current application limits, thorough understanding of the interaction mechanism is necessary. In the current study, the interaction energetics are determined by putting three major point defects, V_{Li}', $Li_i^{\cdot}$, and $Nb_{Li}^{\cdot\cdot\cdot\cdot}$ at various distances from both the Y-walls and the X-wall. Three major point defects and two distinctive domain walls are identified from previous studies. From the full geometry relaxation, the interaction energetics are determined by looking at the energy difference between the defects near the wall and the defects far away from the wall. Although the size limitation constrains the maximum distance of our study at 6.46 Å for the Y-wall and at 7.75 Å for the X-wall, empirical study with a larger system proves that the defects/domain-wall interactions mainly occur within 5 Å.[31] Because the interaction between the defects and the domain wall means that their energies cannot be uniquely separated from each other, we here ascribe the change in the energy of the system to a change in the defect formation energy; we could, with equal merit, ascribe this energy change to a change in the domain wall energy.

Figure 1 provides a schematic view of the Y-wall in $LiNbO_3$ and the spatial location of each point defect near the Y-wall. As can be seen, the Y-wall sits between two atom planes; point defects are located at different distances from the domain walls. For all cases, the defect/domain wall interactions decreased the energy, indicating that defects are preferentially positioned near the domain wall. For the Y-wall, the quadrupley charged $Nb_{Li}^{\cdot\cdot\cdot\cdot}$ shows a stronger interaction (~ –0.26 eV), while the singly charged V_{Li}' or $Li_i^{\cdot}$ shows weaker interaction (~ –0.12 eV). The singly charged defects are preferentially located at the nearest plane from the Y-wall, while the $Nb_{Li}^{\cdot\cdot\cdot\cdot}$ prefer to be at the second nearest plane from the wall. For comparison, the energetics of the neutral defects are also considered. Interestingly, three neutral defects show similar energetics regardless of their kinds and the values are quite close to the case of the singly charged defects (V_{Li}^{x} = ~ –0.11 eV, Li_i^{x} = ~ –0.12 eV and Nb_{Li}^{x} = ~ –0.14 eV). Thus, the charge states of defects play an important role in determining the energetics for the defect/Y-wall interactions.

A similar study has been also performed for the X-walls. Because our previous study identified two inequivalent X-walls related with the oxygen sublattice, current studies have calculated the interaction energies of intrinsic defects with both the X_I-*wall* and the X_{II}-*wall*. Although maximum interactions are observed within the second nearest plane from both the X-walls regardless of the charge states of the intrinsic defects, the energetics for their interactions are different. Fig. 2 shows a comparison of the maximum defects/X-wall interaction energy within the three nearest planes. As can be seen in Fig. 2, the majority of defects show stronger interaction with the X_I-*wall* than with the X_{II}-*wall*. The most prominent difference in the interaction energetics is observed for the quadrupley charged $Nb_{Li}^{\cdot\cdot\cdot\cdot}$. The DFT predicts that the interaction of $Nb_{Li}^{\cdot\cdot\cdot\cdot}$ with the X_I-*wall* (~ –0.55 eV) will be much stronger than that with the X_{II}-*wall* (~ –0.05 eV). For single charged defects, the maximum interaction energies of $Li_i^{\cdot}$ are –0.32 eV for the X_I-*wall* and –0.16 eV for the X_{II}-*wall;* the maximum interaction energies of V_{Li}' are –0.14 eV for the X_I-*wall* and –0.13 eV for the X_{II}-*wall*. Similar to the fully charged defects, the X_I-*wall* also shows stronger interaction with neutral defects; the value of –0.17 eV of the Nb_{Li}^{x} /X_I-*wall* interaction energy is stronger than the value of –0.03 eV of the Nb_{Li}^{x}/X_{II}-*wall* interaction energy. Previous study identified that two inequivalent X-walls have essentially identical values of domain wall

energy in a perfect system. With the existence of defects, however, the current study observed that the X_I-*wall* could be energetically more stable than the X_{II}-*wall*. Thus, the defects/X-walls interactions explain the experimental preference of the X_I-*wall* over the X_{II}-*wall*.[16,19]

Previous study has shown that the domain wall in $PbTiO_3$[32] acts as a trap site for oxygen vacancies. As an extension of that study, the current work shows that the domain wall does not act as a trap site for only oxygen vacancies, but for all other intrinsic defects regardless of their charge states or defect types. For the Y-wall, the quadrupely charged $Nb_{Li}^{\cdots\cdot}$ will more strongly interact with the wall than the singly charged $V_{Li}^{'}$ and $Li_i^{\cdot}$. On the other hand, $Li_i^{\cdot}$. and $Nb_{Li}^{\cdots\cdot}$ should interact more strongly with the X_I-*wall* than with the X_{II}-*wall*. Because the strong interaction of $Nb_{Li}^{\cdots\cdot}$ with the domain walls increases the stability of the domain wall, the domain wall motion will be more difficult with the existence of $Nb_{Li}^{\cdots\cdot}$. Thus, among the three intrinsic defects, $Nb_{Li}^{\cdots\cdot}$ will show the strongest pinning effect .

Because the domain walls act as trap sites for defects, defects might form a cluster near the domain walls. In order to verify the energetics of single defect/domain wall interactions, we have also considered defect clusters. For this study, we have considered two different defect pairs, $Li_i^{\cdot}+V_{Li}^{'}$ and $Nb_{Li}^{\cdots\cdot}+4V_{Li}^{'}$. By assuming that defects do not interact with each other and are equally distant from the wall, we were able to determine the maximum interaction energy of the two defect clusters with one Y-wall and two X-walls; the defect cluster/domain wall interaction energies are shown in the change of DFE from the reference state and listed in Table 1. Consistent with the results of the single defect case, three different types of domain walls act as trap sites for both defect pairs. Also, the X_I-*wall* interacts more strongly with both defect clusters.

We have looked at the energetics of the defects interacting with domain walls in $LiNbO_3$. Now we will discuss how the defects can migrate near the domain wall. In order to study the migration of various point defects, we have employed the NEB method along the migration pathway. Because the previous study[17] has shown that the Y-wall, lying parallel to the $(11\bar{2}0)$ plane, is energetically much more favorable than the two X-walls, our study focused on the migration behavior of defects around the Y-wall. Especially, the current study has focused on the $Nb_{Li}^{\cdots\cdot}$-$V_{Li}^{'}$ pair, because $Nb_{Li}^{\cdots\cdot}$ is the most highly interacting type of defect and $V_{Li}^{'}$ is necessary for mitigating the highly positive charge state of $Nb_{Li}^{\cdots\cdot}$. Fig. 3 shows the potential energy profile along the migration pathway of the $Nb_{Li}^{\cdots\cdot}$-$V_{Li}^{'}$ pair across the Y-wall. The bottom figures show the atomic configuration of the $Nb_{Li}^{\cdots\cdot}$-$V_{Li}^{'}$ pair across the Y-wall in the initial state (IS),

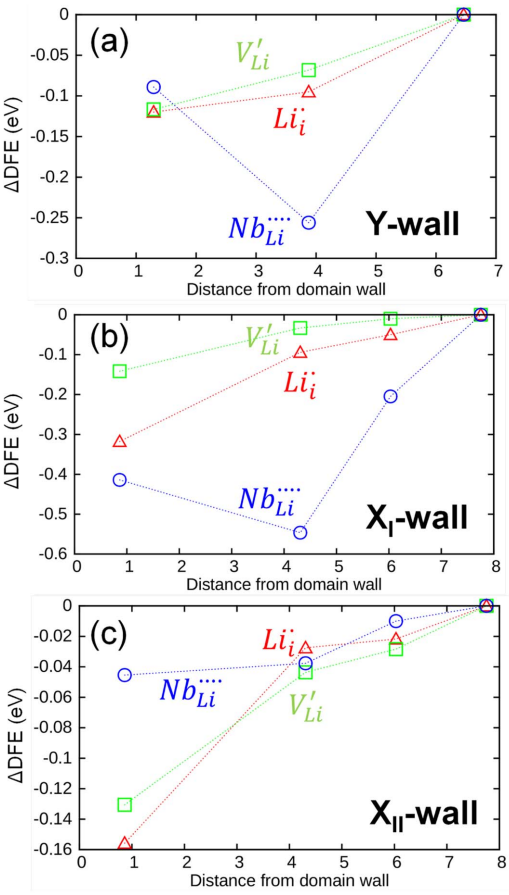

Fig. 2. Variation of defect formation energy (DFE) as a function of distance from (a) Y-wall, (b) X_I-*wall* and (c) X_{II}-*wall*. The DFE of three dominant point defects: $Li_i^{\cdot}$ (red), $V_{Li}^{'}$ (green) and $Nb_{Li}^{\cdots\cdot}$ (blue) are calculated using density functional theory (DFT).

Table 1. Comparison of Interaction Energies of Two Defect Complexes with One Y-wall and two X-walls. The DFE at Bulk State is Shown as a Reference for Each Configuration

	DFE at bulk	Y-wall	X_I-wall	X_{II}-wall
$Li_i^{\cdot}+V_{Li}^{'}$	0.75	-0.12	-0.23	-0.14
$Nb_{Li}^{\cdots\cdot}+4V_{Li}^{'}$	-1.00	-0.15	-0.22	-0.11

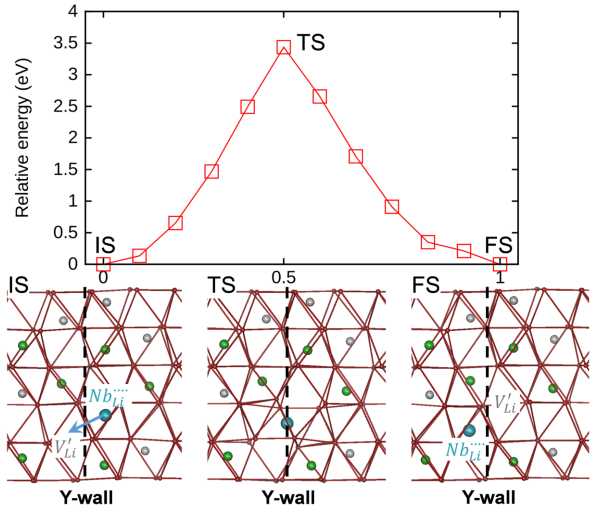

Fig. 3. Potential energy profile along the migration pathway of the $V_{Li}^{'}/Nb_{Li}^{\cdots\cdot}$ pair across the Y-wall.

transition state (TS) and final state (FS). As can be seen, $Nb_{Li}^{\cdots\cdot}$ and $V_{Li}^{'}$ sit in two oxygen octahedral cages across the Y-wall that are next to each other. Thus, it is reasonable to assume that $Nb_{Li}^{\cdots\cdot}$ will migrate through the shortest pathway to $V_{Li}^{'}$, as shown by the cyan arrow in the left bottom of Fig. 3. The migration barrier for $Nb_{Li}^{\cdots\cdot}$ moving toward the $V_{Li}^{'}$ site is 3.44 eV at the transition state (TS). This shows that significant energy is required to move $Nb_{Li}^{\cdots\cdot}$ across the Y-wall. Therefore, it is reasonable to think that $Nb_{Li}^{\cdots\cdot}$, which can be easily captured by the Y-wall, will have difficulty migrating across the Y-wall and thus will pin the Y-wall.

We now consider how the migration behavior of the $Nb_{Li}^{\cdots\cdot}$-$V_{Li}^{'}$ pair changes under surplus electrons. Fig. 4 shows the potential energy profile along the migration pathway of the $Nb_{Li}^{\cdots\cdot}$-$V_{Li}^{'}$ pair under one excess electron.

The addition of an extra electron decreases the migration barrier of the $Nb_{Li}^{\cdots\cdot}$-$V_{Li}^{'}$ pair from 3.44 to 3.16 eV. Thus, the extra electron will enhance the migration of $Nb_{Li}^{\cdots\cdot}$ into $V_{Li}^{'}$. In order to understand the decrease in the migration barrier of $Nb_{Li}^{\cdots\cdot}$ into $V_{Li}^{'}$, the electronic density of state (DOS) is analyzed. The inset of Fig. 4 shows the site projected DOS at the TS during the migration of $Nb_{Li}^{\cdots\cdot}$ into $V_{Li}^{'}$. At the TS, $Nb_{Li}^{\cdots\cdot}$ sits exactly on the Y-wall. (See Fig. 3) As a result, a defect energy level is created near the conduction band minimum (CBM) of bulk $LiNbO_3$. This energy level created by $Nb_{Li}^{\cdots\cdot}$ is shown in red color in the DOS. We term this energy level a gap state because it is located within the bandgap of bulk $LiNbO_3$. This gap state plays a major role in the change in energy barrier during the migration of $Nb_{Li}^{\cdots\cdot}$. At the IS, $Nb_{Li}^{\cdots\cdot}$ does not yield any defect energy level within the bandgap. On the other hand, $Nb_{Li}^{\cdots\cdot}$, which sits in the Y-wall, will create an additional gap state at the TS. Because this gap state is only available at the TS, extra electrons will go to the bottom of the conduction band at the IS. In contrast, the peeling off of a gap state from the bottom of the conduction band reduces the energy of the system at the TS of the $Nb_{Li}^{\cdots\cdot}$-$V_{Li}^{'}$ migration. Thus, the migration barrier of the $Nb_{Li}^{\cdots\cdot}$-$V_{Li}^{'}$ pair is reduced by the addition of an electron. Because $Nb_{Li}^{\cdots\cdot}$ can pin the motion of the Y-wall, the reduction of the migration barrier of $Nb_{Li}^{\cdots\cdot}$ may enhance the movement of the Y-wall by weakening the pinning effect.

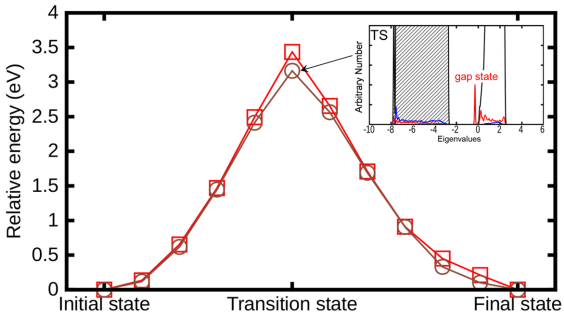

Fig. 4. Potential energy profile along the migration pathway of $V^{'}/Nb_{Li}^{\cdots\cdot}$ pair under influence of one extra electron.

4. Conclusions

Current works have performed a systematic study of the energetics of defects/domain wall interaction in $LiNbO_3$. Our energetic study predicts that the formation energy of intrinsic defects can be lowered near the domain wall. So, the interactions of intrinsic point defects with domain walls decrease the DFE and trap the defects in the domain wall. In the following study, we find that the migration barrier of $Nb_{Li}^{\cdots\cdot}$ is significantly high near the Y-wall. Thus, the trapped defects increase the coercive energy and threshold field for the domain wall motion, in what is known as the pinning effect. In addition, trapped defects can cause a local field and this might cause optical degradation. The degradation in both ferroelectricity and the optical property is known as ferroelectric fatigue. By identifying the defects and defect pairs leading to the strongest interaction with the domain walls, we can potentially prevent ferroelectric fatigue or optical degradation by constraining the formation of specific types of defect. From our systematic study of defect/domain interactions, the current works show that $Nb_{Li}^{\cdots\cdot}$ has the strongest interaction with both one Y-wall and two X-walls. Therefore, reducing or replacing $Nb_{Li}^{\cdots\cdot}$ with low interacting defects may be one way to overcome the known limitations of ferroelectric $LiNbO_3$.

Acknowledgments

This work was supported by Chonnam National University, 2015, and by the National Institute of Supercomputing and the Network/Korea Institute of Science and Technology Information with supercomputing resources including technical support, No. KSC-2015-C3-034.

REFERENCES

1. D. G. Lim, B. S. Jang, S. I. Moon, C. Y. Won, and J. Yi, "Characteristics of $LiNbO_3$ Memory Capacitors Fabricated Using a Low Thermal Budget Process," *Solid-State Electron.*, **45** [7] 1159-63 (2001).
2. J. Macario, P. Yao, R. Shireen, C. A. Schuetz, S. Y. Shi, and D. W. Prather, "Development of Electro-Optic Phase Modulator for 94 GHz Imaging System," *J. Lightwave Technol.*, **27** [24] 5698-703 (2009).
3. A. Tehranchi and R. Kashyap, "Efficient Wavelength Converters with Flattop Responses Based on Counterpropagating Cascaded SFG and DFG in Low-Loss QPM $LiNbO_3$ Waveguides," *Opt. Express,* **17** [21] 19113-19 (2009).
4. K. K. Wong, "Properties of Lithium Niobate," EMIS Datareviews, 28, INSPEC, The Institution of Electrical Engineers, United Kingdom, Lon-don, 2002.
5. T. Volk and M. Wöhlecke, "Lithium Niobate: Defects, Photo-refraction and Ferroelectric Switching," Springer Series in MATERIALS SCIENCE, 115, Springer, Berlin, 2008.
6. Y. H. Han and D. M. Smyth, "Nonstoichiometry and Defects in Linbo3," *Am. Ceram. Soc. Bull.*, **62** [8] 852

(1983).
7. H. M. Obryan, P. K. Gallagher, and C. D. Brandle, "Congruent Composition and Li-Rich Phase-Boundary of LinbO_3," *J. Am. Ceram. Soc.*, **68** [9] 493-96 (1985).
8. P. F. Bordui, R. G. Norwood, D. H. Jundt, and M. M. Fejer, "Preparation and Characterization of Off-Congruent Lithium-Niobate Crystals," *J. Appl. Phys.,* **71** [2] 875-79 (1992).
9. N. Iyi, K. Kitamura, F. Izumi, J. K. Yamamoto, T. Hayashi, H. Asano, and S. Kimura, "Comparative-Study of Defect Structures in Lithium-Niobate with Different Compositions," *J. Solid State Chem.*, **101** [2] 340-52 (1992).
10. W. Bollmann, "Stoichiometry And Point-Defects in Lithium-Niobate Crystals," *Cryst. Res. Technol.,* **18** [9] 1147-49 (1983).
11. O. F. Schirmer, O. Thiemann, and M. Wohlecke, "Defects in linbo3 .1. Experimental Aspects," *J. Phys. Chem. Solids,* **52** [1] 185 (1991).
12. H. Donnerberg, S. M. Tomlinson, C. R. A. Catlow, and O. F. Schirmer, "Computer-Simulation Studies of Intrinsic Defects in LinbO_3 Crystals," *Phys. Rev. B,* **40** [17] 11909 (1989).
13. H. X. Xu, D. Lee, J. He, S. B. Sinnott, V. Gopalan, V. Dierolf, and S. R. Phillpot, "Stability of Intrinsic Defects and Defect Clusters in $LiNbO_3$ from Density Functional Theory Calculations," *Phys. Rev. B,* **78** [17] 174103 (2008).
14. H. X. Xu, D. Lee, S. B. Sinnott, V. Dierolf, V. Gopalan, and S. R. Phillpot, "Structure and Diffusion of Intrinsic Defect Complexes in $LiNbO_3$ from Density Functional Theory Calculations," *J. Phys.: Condens. Matter,* **22** [13] 135002 (2010).
15. V. Gopalan, V. Dierolf, and D. A. Scrymgeour, "Defect-Domain Wall Interactions in Trigonal Ferroelectrics," *Annu. Rev. Mater. Res.*, **37** 449-89 (2007).
16. D. A. Scrymgeour, V. Gopalan, A. Itagi, A. Saxena, and P. J. Swart, "Phenomenological Theory of a Single Domain Wall in Uniaxial Trigonal Ferroelectrics: Lithium Niobate and Lithium Tantalate," *Phys. Rev. B,* **71** [18] 184110 (2005).
17. D. Lee, H. Xu, V. Dierolf, V. Gopalan, and S. R. Phillpot, "Structure and Energetics of Ferroelectric Domain Walls in $LiNbO_3$ from Atomic-level Simulations," *Phys. Rev. B,* **82** [1] 014104 (2010).
18. D. Lee, R. K. Behera, P. Wu, H. X. Xu, S. B. Sinnott, S. R. Phillpot, L. Q. Chen, and V. Gopalan, "Mixed Bloch-Néel-Ising Character of 180° Ferroelectric Domain Walls," *Phys. Rev. B,* **80** [6] 060102(R) (2009).
19. D. Lee, H. Xu, V. Dierolf, V. Gopalan, and S. R. Phillpot, "Shape of Ferroelectric Domains in $LiNbO_3$ and $LiTaO_3$ from Defect/Domain-Wall Interactions," *Appl. Phys. Lett.*, **98** [9] 092903 (2011).
20. G. Stone, D. Lee, H. Xu, S. R. Phillpot, and V. Dierolf, "Local Probing of the Interaction between Intrinsic Defects and Ferroelectric Domain Walls in Lithium Niobate," *Appl. Phys. Lett.*, **102** [4] 042905 (2013).
21. W. Kohn and L. J. Sham, "Self-Consistent Equations Including Exchange And Correlation Effects," *Phys. Rev.*, **140** [4A] A1133 (1965).
22. J. P. Perdew and W. Yue, "Accurate and Simple Density Functional For The Electronic Exchange Energy - Generalized Gradient Approximation," *Phys. Rev. B,* **33** [12] 8800 (1986).
23. H. J. Monkhorst and J. D. Pack, "Special Points for Brillouin-Zone Integrations," *Phys. Rev. B,* **13** [12] 5188 (1976).
24. G. Kresse and J. Furthmuller, "Efficiency of ab-initio Total Energy Calculations for Metals and Semiconductors Using a Plane-Wave Basis Set," *Comput. Mater. Sci.*, **6** [1] 15-50 (1996).
25. G. Kresse and J. Furthmuller, "Efficient Iterative Schemes for ab Initio Total-Energy Calculations Using a Plane-Wave Basis Set," *Phys. Rev. B,* **54** [16] 11169 (1996).
26. P. E. Blochl, "Projector Augmented-Wave Method," *Phys. Rev. B*, **50** [24] 17953 (1994).
27. Q. K. Li, B. Wang, C. H. Woo, H. Wang, and R. Wang, "First-Principles Study on the Formation Energies of Intrinsic Defects in $LiNbO_3$," *J. Phys. Chem. Solids*, **68** [7] 1336-40 (2007).
28. P. Pulay, "Convergence Acceleration Of Iterative Sequences - The Case Of Scf Iteration," *Chem. Phys. Lett.*, **73** [2] 393-98 (1980).
29. H. Jónsson, G. Mills, and K. W. Jacobsen, "Nudged Elastic Band Method for Finding Minimum Energy Paths of Transitions," CLASSICAL AND QUAN-TUM DYNAMICS IN CONDENSED PHASE SIMULATIONS, pp. 385, World Scientific, 1998.
30. G. Henkelman, B. P. Uberuaga, and H. Jonsson, "A Climbing Image Nudged Elastic Band Method for Finding Saddle Points and Minimum Energy Paths," *J. Chem. Phys.,* **113** [22] 9901-4 (2000).
31. D. Lee, Structure and dynamics of interfaces in organic and inorganic materials using atomic level simulation (*in English*), pp. 111 in Ph.D. Thesis, University of Florida, Gainesville, Fl, 2010.
32. L. He and D. Vanderbilt, "First-Principles Study of Oxygen-Vacancy Pinning of Domain Walls in $PbTiO_3$," *Phys. Rev. B*, **68** [13] 134103 (2003).